Journal of Hazardous Materials 458 (2023) 131849

Contents lists available at ScienceDirect

Journal of Hazardous Materials

journal homepage: www.elsevier.com/locate/jhazmat

Mechanistic insights into Pb and sulfates retention in ordinary Portland cement and aluminous cement: Assessing the contributions from binders and solid waste

Yikai Liu [a], Simone Molinari [a,*], Maria Chiara Dalconi [a], Luca Valentini [a], Maurizio Pietro Bellotto [b], Giorgio Ferrari [c], Roberto Pellay [d], Graziano Rilievo [e], Fabio Vianello [e], Gabriella Salviulo [a], Qiusong Chen [f,g], Gilberto Artioli [a]

[a] Department of Geosciences and CIRCe Centre, University of Padua, via G. Gradenigo 6, 35129 Padua, Italy
[b] OPIGEO Srl, Montegalda, Vicenza, Italy
[c] Mapei S.p.A., via Cafiero 22, 20158 Milan, Italy
[d] TEVGroup S.r.l., via Romea 8, Mira, 30034 Venice, Italy
[e] Department of Comparative Biomedicine and Food Science, University of Padova, Viale dell'Università 16, 35020 Legnaro, Italy
[f] Sinosteel Maanshan General Institute of Mining Research Co., Ltd., Maanshan 24300, China
[g] School of Resources and Safety Engineering, Central South University, Lushan South Road 932, 410083 Hunan, China

HIGHLIGHTS

- A geochemical model with an adsorption parameter fitting function was developed.
- Provide an in-depth understanding of Pb and sulfate retention in a broad pH range.
- The competitiveness of precipitation and sorption for Pb retention was clarified.
- Aluminous cement showed relatively high compatibility with Pb immobilization.

GRAPHICAL ABSTRACT

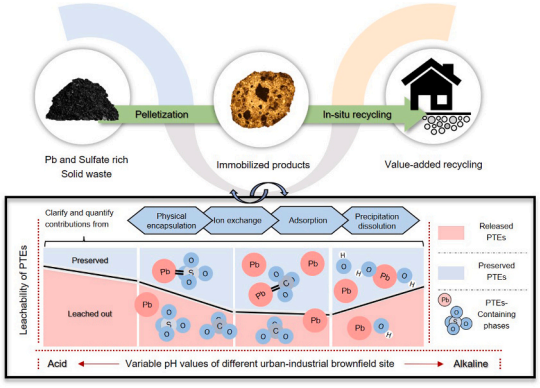

ARTICLE INFO

Editor: John D Atkinson

Keywords:
Potentially toxic elements
Solidification/stabilization
Cement

ABSTRACT

Identifying immobilization mechanisms of potentially toxic elements (PTEs) is of paramount importance in the field application of solidification/stabilization. Traditionally, demanding and extensive experiments are required to better access the underlying retention mechanisms, which are usually challenging to quantify and clarify precisely. Herein, we present a geochemical model with parametric fitting techniques to reveal the solidification/stabilization of Pb-rich pyrite ash through conventional (ordinary Portland cement) and alternative (calcium aluminate cement) binders. We found that ettringite and calcium silicate hydrates exhibit strong affinities for Pb

* Corresponding author.
E-mail address: simone.molinari@unipd.it (S. Molinari).

https://doi.org/10.1016/j.jhazmat.2023.131849
Received 3 April 2023; Received in revised form 31 May 2023; Accepted 12 June 2023
Available online 17 June 2023

Geochemical modelling
Pyrite ash

at alkaline conditions. When the hydration products are unable to stabilize all the soluble Pb in the system, part of the soluble Pb may be immobilized as $Pb(OH)_2$. At acidic and neutral conditions, hematite from pyrite ash and newly-formed ferrihydrite are the main controlling factors of Pb, coupled with anglesite and cerussite precipitation. Thus, this work provides a much-needed complement to this widely-applied solid waste remediation technique for the development of more sustainable mixture formulations.

1. Introduction

The stockpiling of potentially toxic elements (PTEs) containing solid waste is an inevitable consequence of global anthropogenic activities and has become one of the most widespread and critical problems worldwide [74,78]. Many works have shown that the excessive accumulation of PTEs can cause carcinogenic and poisoning effects on biota, thus harming ecosystems [65,67]. For instance, the intake of Pb can cause various life-threatening cancers [40], and the over-inhalation of sulfates may impair human taste and induce diarrhoea [69]. Considering the ubiquitous presence of PTEs in the earth's upper crust [43], many attempts have been made to devise management strategies aimed at avoiding the occasional inhalation or inadvertent ingestion of these contaminants.

In this light, the in-situ solidification/stabilization (S/S) approach is recognized as an efficient and practicable remediation strategy with great potential to be extrapolated in field trials [14,31]. Generally, ordinary Portland cement (OPC) represents the prevailing binder extensively used in the S/S process [30], but recent studies within this decade have highlighted the importance of mitigating the use of OPC in order to entail reaching low CO_2 emissions [10,18,79]. Especially, the OPC-based mixtures are fairly sensitive to the pH variabilities. Many works have proven that PTEs release can significantly increase when the pH value of OPC-based mixtures lowers toward neutral conditions as a consequence of weathering process or atmospheric carbonation [17,52]. Therefore, a growing body of evidence has shown that developing alternative low-carbon and highly efficient binders is a crucial way to reduce the CO_2 emission related to the S/S process, as well as facilitating the PTEs immobilization [9]. Many researchers have raised ever-increasing attention to the use of alternative materials for PTEs immobilization, such as kaolinite [14], biochar [75], calcium aluminate cement (CAC) [8], granulated blast furnace slag [73]. However, unlike the well-established OPC system, the controls of PTEs in systems based on alternative cement remain poorly known [39]. The PTEs fate is still a matter of debate despite it is well known that the S/S process diminishes the mobility of the toxic elements predominantly in two manners (1) coprecipitation and adsorption by hydration products and (2) micro- or macro-encapsulation and chemical fixation [54]. More importantly, the binder-waste assemblage is highly sensitive to the pH values, which are controlled by many factors, such as the mineralogical composition, the dissolution of the PTEs-bearing phases (e.g., Pb hydroxides and Zn hydroxides), and the interaction with percolating rainwater [1,79]. Furthermore, the Pb leaching at acid conditions could be several magnitudes (10^4 or 10^5) higher than in neutral pH conditions [14]. Therefore, characterizing the PTEs leaching behaviors and the associated mechanisms over a broad pH range is fundamental in tailoring the field application [14,50]. However, relevant empirical analysis to reveal the underlying mechanisms responsible for the leaching behavior of constituents remains poorly understood.

Based on several recent studies, the geochemical modeling approach could disentangle how this coupling operates, where insights can be gained through the use of pH-dependent leaching tests in association with geochemical speciation modeling [12,23,41,66]. In systemic studies, the dissolution/precipitation equilibrium of the PTEs-containing phases and the cementitious assemblages is assumed to be the primary mechanism for the leaching behavior of the PTEs. However, there is strong evidence that the ion exchange and adsorption also play a critical role in controlling the PTEs release, for instance, the Pb could be incorporated into the ettringite structure [15] and adsorbed onto the surface of C-S-H/C-A-S-H gel [9,44]. The reconstruction of these processes in geochemical modeling is still fragmented and poorly constrained [70,80]. This is because the representativeness of the modeling is limited by the amount of available data from the thermodynamic database [38,48]. These knowledge gaps hinder the development of a fundamental understanding of the controls on PTEs release and migration.

To contribute to filling in these gaps, the main objectives of this work are: (1) elucidating the roles of traditional (OPC) and alternative (CAC) binders in Pb retention, thus addressing the relatively low Pb immobilization efficiency associated with conventional OPC and (2) integrating the insights into the adsorption and ion exchange mechanisms controlling Pb mobilization. To achieve these goals, pyrite ash (PA) was characterized to explore its mineralogical composition and the source of Pb. Subsequently, the Pb retention performance of S/S immobilized PA in both traditional and alternative ways was evaluated by X-ray diffraction (XRD) analyses, scanning electron microscopy/energy dispersive spectroscopy (SEM/EDS) investigation, and pH-dependent leaching tests. Further, the PA-binder assemblages after the leaching tests were collected to quantify mineral phase dissolution and re-precipitation. Finally, with the thorough characterization of the partitioning of chemical species, we constructed geochemical modeling coupled with the Parameter Estimation software (PEST). By comparing the identified PTEs' leaching behavior from experiment and simulation, we investigated and quantitatively classified the impacts from dissolution/precipitation, adsorption, and physical encapsulation on Pb capture. The results of this paper demonstrate the feasibility of using the Portland-free pathway to immobilize the PA. Further, it provides a reliable methodology to guide and test the plausibility of conceptual and numerical models of Pb mobilization and transport, even with a limited dataset, which may contribute to a more complete picture of PTEs release mechanisms in the stabilized products and improve the trail application of S/S technologies.

2. Materials and methods

2.1. Sampling and pelletization process

The PA is collected from an abandoned factory in Ancona, Italy, which was devoted to the pyrite (FeS_2) roasting process to produce sulfuric acid. This site is currently used to store solid waste from the pyrite roasting process, sulphuric acid production, and fertilizer production. Samples were collected on a systematic sampling grid from the surface to a depth of 2.5 m, covering an area of approximately 0.11 km^2. Before implementing the S/S process, the sample was air-dried and passed through a 2 mm mesh sieve. The binders used in this work are OPC (CEM I 42.5 R, Barbetti S.p.A., Italy) and CAC (Gorkal 40, Mapei S.p.A., Italy). The high-performance S/S process® [14,4] was applied to pelletize the PA and binder. The exact mixture proportion is given in

Table1
The components proportion of pellets (wt%).

Label	PA (dry)	OPC (dry)	CAC (dry)	Water	Water/Solid ratio
OPP	65.2	16.4	-	18.4	0.23
CAP	64.9	-	16.3	18.8	0.23

*Note: the solid represents the total mass of binder (OPC or CAC) and PA

Table1, with the water-to-solid (binder+PA) ratio being kept at 0.23, which is within the typical range (approximately 0.2) in the S/S process for contaminated solid matrices [76]. After pelletization, the samples were sealed in plastic bags for 28 days under ambient conditions and then sieved to a diameter range between 2 and 10 mm (Fig.S1). The chemical compositions of PA, OPC, and CAC are provided in Table.S3.

2.2. Characterization methods

The mineral phases of selected samples were identified by X-ray diffraction (Malvern Panalytical X'Pert Pro diffractometer, UK) with a step of 0.02° and a scanning range of 3–84° 2θ. Samples were ground in an agate mortar and micronized in a McCrone micronizing mill for 5 mins. To quantify the amorphous content in the pellets, 10 wt% of zincite (ACS Reagent, Thermo Fisher Scientific Inc., Waltham, USA) was mixed with the powdered samples as an internal standard. Rietveld refinement of samples was performed with Topas (v2.1), using the Rietveld-Reference Intensity Ratio methods [29,60]. SEM/EDS investigation (CamScan MX3000, Applied Beams, USA) was performed on the polished and carbon-coated PA, OPP, and CAP samples. The X-ray fluorescence characterizations were carried out to determine the elemental composition (PW1480, Philips, USA).

2.3. Leaching procedures and ions concentration determination

The pH-dependent leaching tests were performed on the sieved OPP and CAP samples following the EN 14429:2015 (British Standards Institution, 2015) standard, consisting of a series of parallel batch extractions tests with increasing pH values. Around 4.50 g of sieved OPP and CAP samples were added to 48 mL of ultrapure water (Genie Direct-Pure water device, RephiLe Bioscience Ltd., Shanghai, China) and put under agitation. Then 2 mL of extraction solution (i.e., either nitric acid (HNO_3, 5 Molarity, Honeywell Fluka, Germany) or sodium hydroxide (NaOH, 5 Molarity, Carlo Erba, Italy) solutions) were progressively added to the samples as follows: 1/3 of the extraction solution volume at the beginning of the agitation, 1/3 of the volume after 30 min, and the last 1/3 after 2 h. Amounts and concentrations of the acid/basic agents used for the pH-dependent leaching tests are given in Fig.S3, as well as the final pH values of the collected leachates. For the reliability of the protocol, the pH variation condition between 44 and 48 h imposed by the standard EN 14429:2015 (i.e., $\Delta pH < 1.5$ units) was confirmed. Lastly, the supernatants were collected, filtered with a 0.45 µm filter and brought to $pH < 2$, necessary for the preservation of the liquid sample and for the ICP-MS elementary analysis (Pb, Al, and SO_4). The residual solid phase of the samples was dried for 6 h at 70 °C prior to the XRD characterization. The leaching tests were carried out at room temperature (25 ± 1 °C), and all samples were analysed in triplicates.

2.4. Geochemical modeling construction

PHREEQC [1,20,57] and PEST+ + [22] software were used to calculate the thermodynamically stable phases and identify the possible retention mechanisms (precipitation, adsorption, and ion exchange) during the leaching tests. The databases applied in this work include the cement-specific database CEMDATA18 [47] and the extended database PHREEQCDAT [1]. A schematic of the developed modeling algorithms is shown in Fig. 1.

The solid phase input used in the simulation, indicating the pellets mineralogical compositions, is based on the XRD quantification results and the SEM/EDS observations of OPP and CAP samples. In addition, nitric acid and sodium hydroxide were added to the solution phases to simulate acid/alkaline buffering in the leaching tests. Using the above-mentioned databases, the equilibrium state of possible Pb-bearing phases in OPP and CAP systems was estimated (Fig. 1b). The PEST+ + was coupled with PHREEQC to simulate the roles of adsorption mechanisms (using diffuse-double-layer surface model [24]) of C-S-H, amorphous

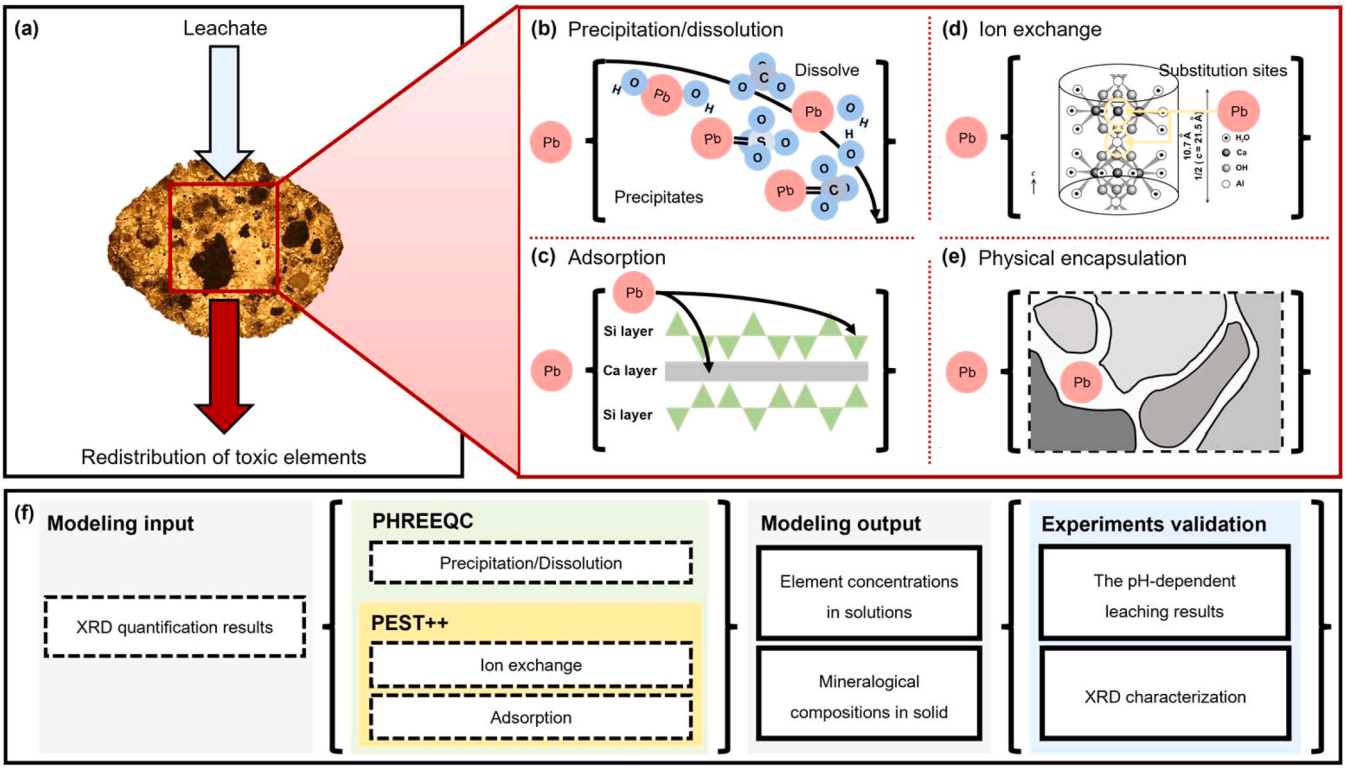

Fig. 1. The Pb retention mechanisms and the framework of the forward modeling construction. (a) the optical microscope image of CAP, (b) precipitation/dissolution of Pb-bearing phases, (c) adsorption of Pb on C-S-H layers, (d) ion exchange of Pb to the ettringite (the ettringite image is from Puppala et al. [58]), (e) physical encapsulation of the Pb, and (f) the simulation framework.

aluminate hydroxide, jarosite, ferrihydrite, and hematite (Fig.S2) and ion exchange mechanisms of ettringite (Fig. 1d) on Pb immobilization [27,30,61]. The output of the coupled model is the concentration of the elements in the leachates, validated by experimental results from the pH-dependent leaching tests and ICP analyses. In addition, the residues of OPP and CAP samples after leaching tests were collected and characterized through XRD to further verify the modeling by comparison with the solid phase compositions in the residues. The Pb/sulfate-containing phase was divided by the initial Pb/sulfate input in the PHREEQC simulation to calculate the changes in Pb/sulfate-containing phase distribution with pH values (e.g., 1 g of total Pb input in the modeling with 0.2 g of Pb precipitates as anglesite, 0.1 g of Pb is adsorbed by C-S-H, and 0.7 g of Pb is the solution, the Pb-containing phases distribution is 20, 10, and 70 wt%).

3. Results

3.1. Characterization of the PA samples

The XRD pattern (Fig. 2a), quantified mineralogical compositions (Table.S3), and SEM/EDS micrograph (Fig. 2b) of PA samples display the typical mineralogical and chemical compositions of roasted pyrite, mainly constituted by hematite (Fe_2O_3), gypsum ($CaSO_4{\cdot}2\,H_2O$) and jarosite ($KFe_3(SO_4)_2(OH)_6$) [53]. Typical silicate minerals, quartz (SiO_2) and feldspar (albite ($NaAlSi_3O_8$), orthoclase ($KAlSi_3O_8$), and/or anorthoclase ((Na, K)$AlSi_3O_8$)) are also present in PA samples. ~~The~~ Pb is mainly present as anglesite ($PbSO_4$) and kintoreite ($PbFe_3(PO_4)(SO_4)(OH)_6$), typical phases usually found in weathered PA [56]. Further, the EDS analyses indicate that aside from anglesite and kintoreite, the presence of Pb in PA is also associated with Ca, Fe, and Si (Fig. 1d) [27]. A detailed characterization of the collected PA samples can be found in our previous work [46].

3.2. Characterization of the OPP and CAP samples

The XRD diffractograms and the quantification results (Fig. 3) show that ettringite is the primary crystalline hydration product (4.5 wt%) detected in the OPP samples. The observed calcite (6.1 wt%) could be attributed to portlandite carbonation at early ages when the cement-based sample is exposed to the ambient atmosphere [63]. By subtracting the known amount of ZnO fraction, the amorphous content is quantified as 24.4 wt%, mainly consisting of the C-S-H gel [14]. Hematite (45.5 wt%), gypsum (9.2 wt%), and jarosite (3.1 wt%), originating from the PA samples, are still present in the stabilized OPP pellets. The Pb-bearing phases demonstrate different fates as the anglesite is totally dissolved, whereas the kintoreite (0.4 wt%) remained in the OPP matrix. Regarding the CAP pellets, large ettringite (14.6 wt %) and gibbsite (4.8 wt%) fractions are present as a consequence of the high Al content of the CAC binder. In turn, the weight percentages of sulfate-bearing minerals, gypsum (4.2 wt%) and jarosite (1.9 wt%) decrease compared to the OPP pellets. The dissolved gypsum and jarosite act as sulfate sources for the ettringite precipitation. Further, the amorphous content in CAP pellets is quantified as 10.0 wt%, which may be primarily attributed to the amorphous $Al(OH)_3$ or CAH gel since the C-(A)-S-H gel does not precipitate in the CAC system [42,59].

The SEM/EDS (Fig.4) images of OPP samples ascertained the presence of unhydrated clinker particles (rectangle-marked particles in Fig.4b) and hematite particles (bright assemblages), which are

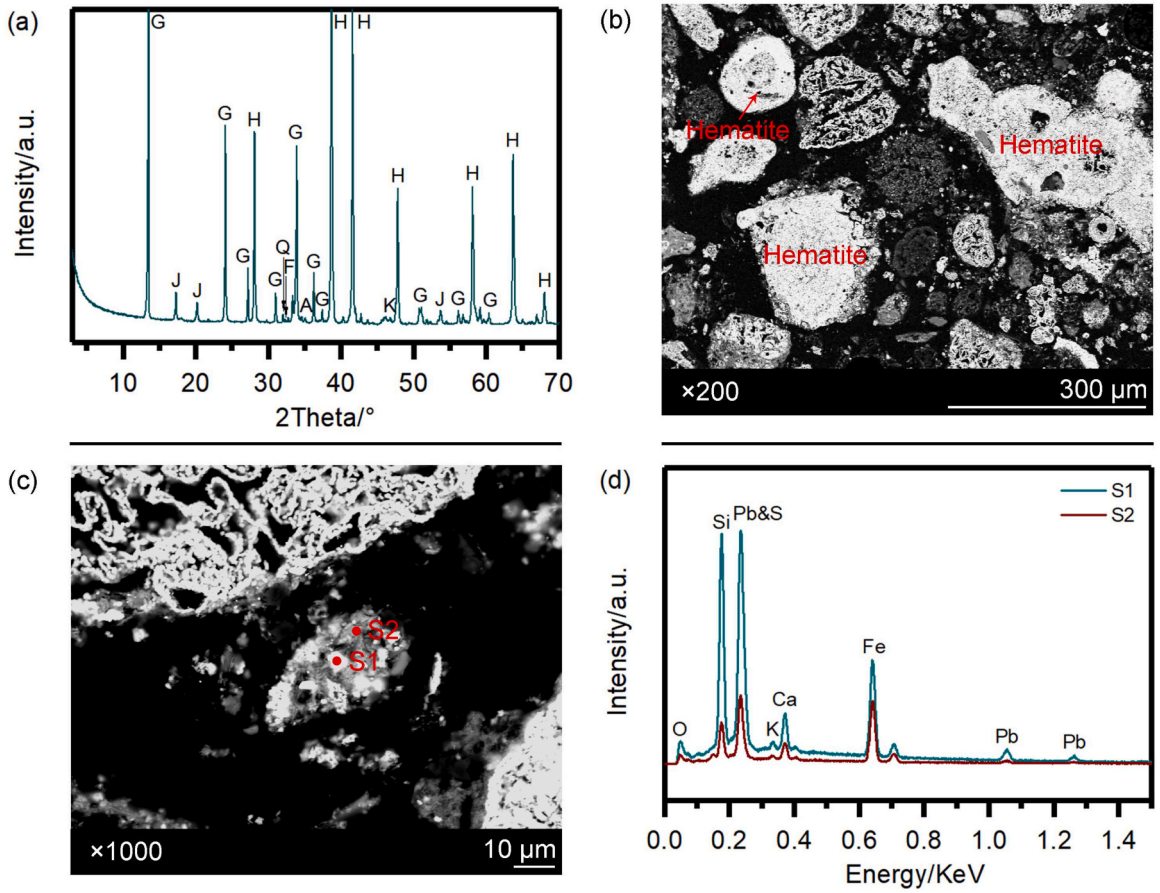

Fig. 2. The mineralogical and BSE images of the PA sample. (a) XRD pattern of the PA powder, (b) BSE image showing the different morphologies of hematite, (c) BSE image demonstrating the Pb incorporation in complexes assemblage, and (d) EDS patterns related to the points marked in image c. A: anglesite, F: feldspar, indicating albite, orthoclase, and/or anorthoclase, G: gypsum, H: hematite, J: jarosite, K: kintoreite, Q: quartz.

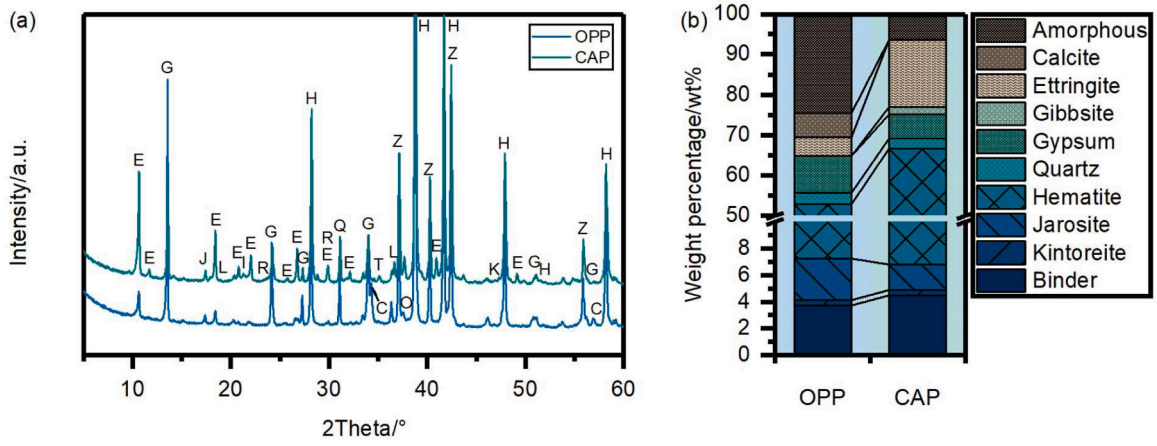

Fig. 3. The XRD investigation of the OPP and CAP samples. (a) XRD patterns and (b) The quantification results. C: calcite, E: ettringite, G: gypsum, H: hematite, I: Gibbsite, J: jarosite, K: kintoreite, L: gehlenite, O: alite and/or belite, Q: quartz, R: grossite, T: krotite, and Z: zincite. Binder in Fig. 2b indicates the sum fraction of alite and belite in OPP samples and the sum fraction of gehlenite, grossite, and krotite in CAP samples.

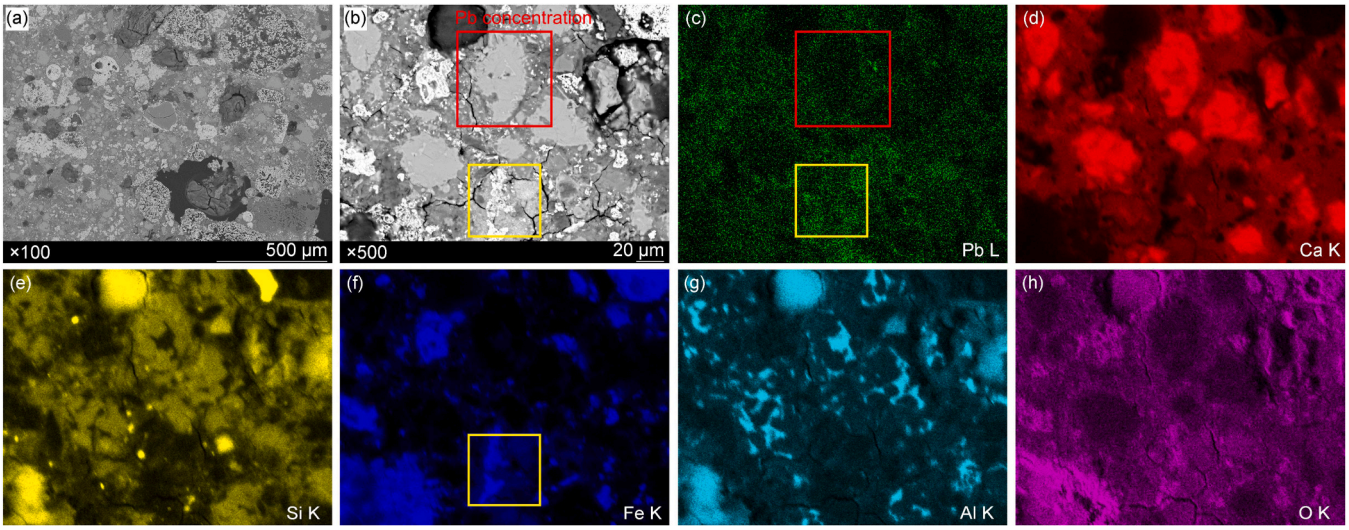

Fig. 4. SEM/BSE images of OPP samples. (a) backscattered microscopy image of OPP sample, (b) images demonstrating the presence of unreacted hematite and clinker phases, (c) elemental mapping of Pb, (d) Ca, (e) Si, (f) Fe, (g) Al, and (h) O.

embedded in the C-S-H matrix (Ca and Si-rich area, see Fig.4d and e) connecting the unreacted portions. Pb (Fig.4c) is homogeneously dispersed within the cementitious matrices, with a slight enrichment along the edge of unhydrated cement particles (red rectangle in Fig.4c) and in the interstitial space of hematite aggregates (yellow rectangle in Fig.4c and f). The presence of Pb in the rims of the unreacted cement particles could be attributed to incorporation in C-S-H through linkages to Si–O chains, which has been widely reported [14,30].

Fig.5a shows the presence of a large amount of ettringite within the cementitious matrix, forming the microstructure of CAP samples. Similar to the OPP samples, Pb was mainly correlated with the hydration products. However, small particles characterized by a marked Pb enrichment can be observed in the matrix (bright particles in Fig.5b and marked circular area in Fig.5c), possibly corresponding to anglesite (Fig.5h). The Si distribution (Fig.5e) is not equal along the different binder scenarios. In CAP samples, it is more relevant to the presence of alkali feldspars solid solutions (e.g., albite, orthoclase, and anorthoclase), originating from the collected PA samples. In addition, Pb is found incorporated in the Fe sulfates aggregates (dash rectangle marked area in Fig.S4a). From the qualitative EDS quantification results (Fig. S4b), the relatively high fraction of Pb (23.8–25.1 wt%), Fe (40.9–42.5 wt%), and S (18.2–19.9 wt%) is compatible with the presence of plumbojarosite ($Pb_{0.5}Fe_3(SO_4)_2(OH)_6$) because the low amount of detected K and Na are not consistent with the presence of potassium/sodium-jarosite ($K/NaFe_3(SO_4)_2(OH)_6$). However, the conditions under which plumbojarosite may form are still not clear. Many studies suggest that this mineral is prone to precipitate and keep stable under harsh acidic conditions with a high-Pb concentration [19,25,36]. But a few field investigations indicate that it can be stable in neutral and basic conditions [26,37,7]. It should be considered that at high pH values and high Ca concentrations, the precipitation of Ca-containing phases (portlandite and/or calcite) can affect the decomposition kinetics of plumbojarosite [37]. In particular, portlandite and calcite tend to preserve the plumbojarosite aggregates and accordingly lower the dissolution rate tend to block the plumbojarosite aggregates and accordingly lower the dissolution rate.

3.3. *Leaching behavior of Pb and sulfates from the pH-dependent leaching tests and modeling*

To reveal the PTEs immobilization efficiency of the OPP and CAP pellets, the leaching behaviors of Pb and sulfates at different pH values

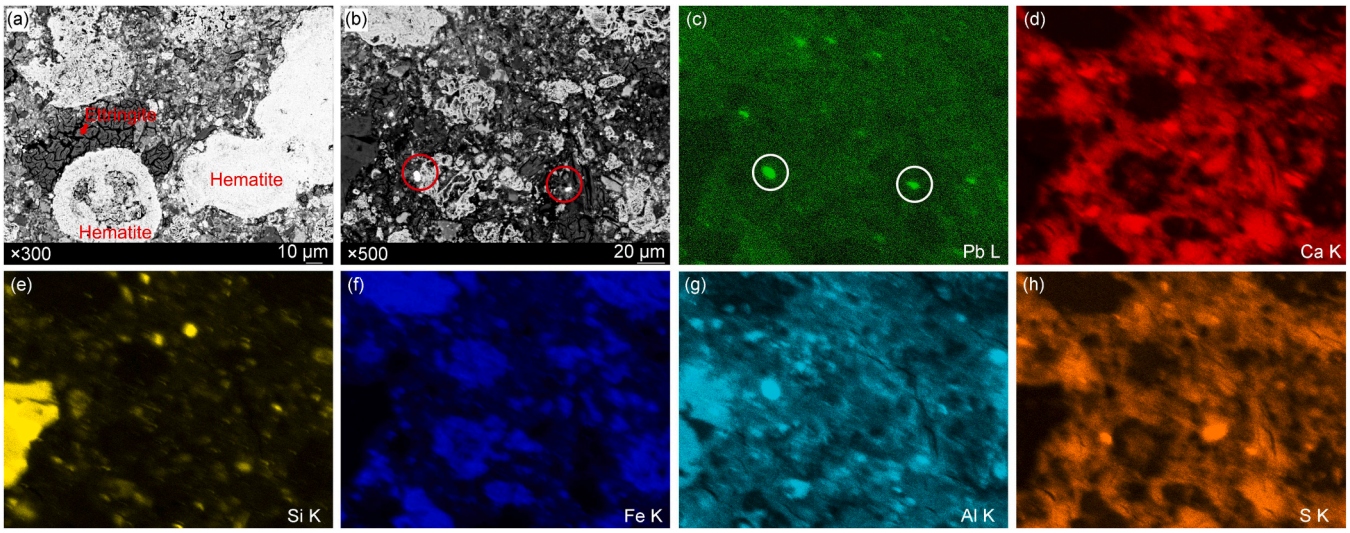

Fig. 5. SEM/BSE images of CAP samples. (a) backscattered microscopy image of CAP sample, (b) image demonstrating the presence of lead sulfates, (c) elemental mapping of Pb, (d) Ca, (e) Si, (f) Fe, (g) Al, and (h) S.

were investigated (Fig.6). The amount of HNO_3 and NaOH solutions used to reach the target pH values are given in Fig.S3. The detected pH value of CAP pellets (pH 9.8) is slightly lower compared to OPP pellets (pH 10.9) and is consistent with results reported in the literature [14,5]. Concerning the Pb leaching (Fig.6a and b), both scenarios show amphoteric leaching behavior, where the minimum Pb leachability of

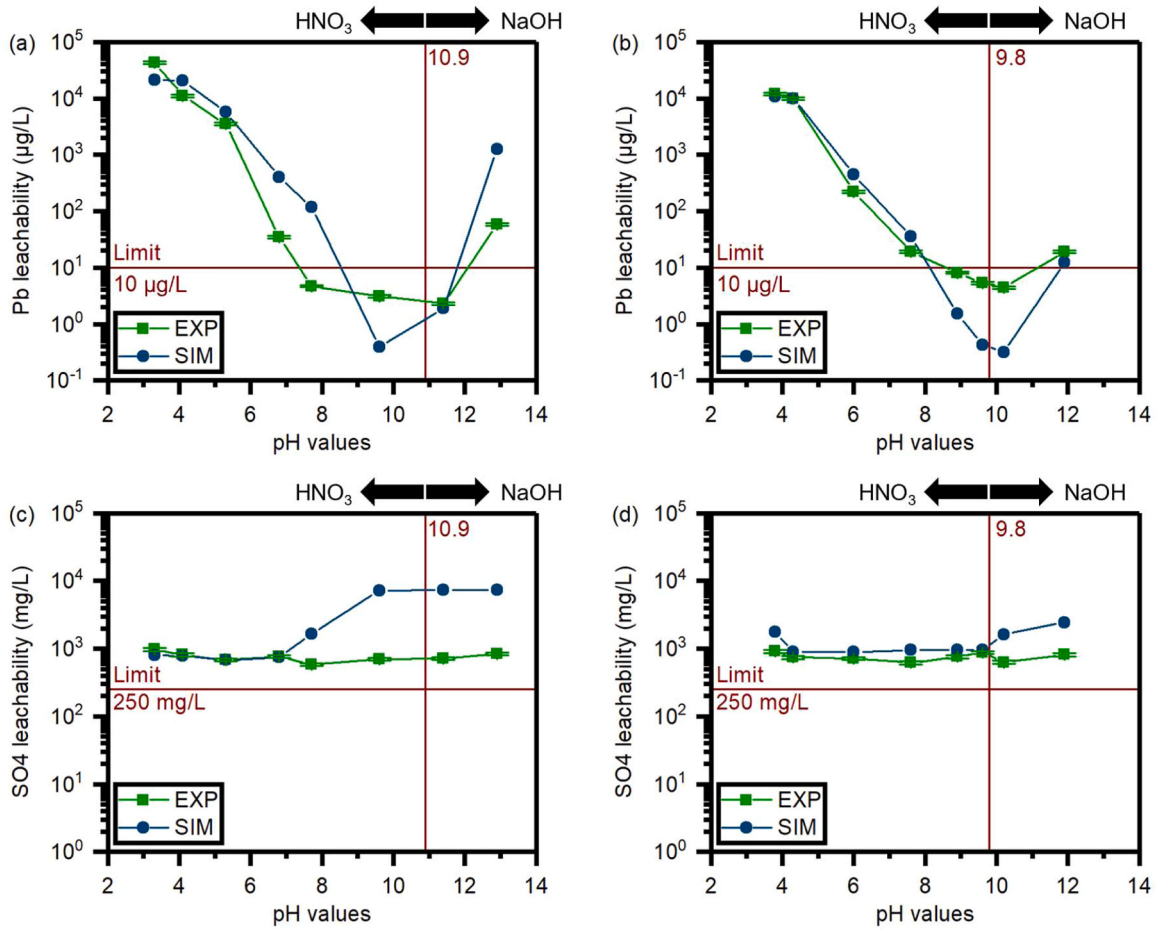

Fig. 6. The pH-dependent leaching tests of Pb and sulfates. (a) The leaching behavior of Pb in OPP samples, (b) The leaching behavior of Pb in CAP samples, (c) The leaching behavior of sulfates in OPP samples, and (d) The leaching behavior of sulfates in CAP samples. EXP and SIM indicate the leaching results from experiments and simulation, respectively. 10.9 and 9.8 solid lines represent the detected pH value of the OPP and CAP pellets, using ultrapure water as the extraction solution. The limits of Pb and sulfate concentration is from Standard based on Decreto legislativo 3 aprile 2006, n. 152, Norme in materia ambientale. HNO_3 and NaOH mean the buffering agent used to reach the target pH values.

OPP (2.3 μg/L) and CAP (4.4 μg/L) pellets were observed at pH 11.4 and 10.2, respectively. Although the Pb retention efficiency of the CAP sample is slightly lower than the traditional OPP sample at moderate alkaline conditions, the Pb retention capacity of CAP at highly-acidic and -alkaline conditions is more satisfactory than the OPP samples. When the pH value decreases below 4, the detected Pb concentration of OPP is 43000 μg/L (pH 3.3), whereas the highest value (12000 μg/L) for CAP was found at pH 3.8. The estimated Pb release from OPP and CAP modeling also ascertained their experimentally determined amphoteric characteristic, as the highest Pb concentration was observed at harsh acid conditions (pH<4) and the lowest is presented at moderate alkaline conditions (pH from 7 to 11).

Contrary to the Pb leaching behavior, the sulfate releasing is close to a steady dissolution state for both scenarios, varying from 600 to 970 mg/L in the studied pH range (Fig.6c and d). However, the simulation of sulfate leaching of OPP samples at basic and neutral conditions is less satisfactory than the estimation at acid conditions. With the increase of pH values, the sulfates concentration from the modeling gradually increased (pH approximately at 7–10) and then remained stable under alkaline conditions, but an order of magnitude higher than the experimental results (e.g., 7.3 $\times 10^3$ and 8.4 $\times$ 10^2 mg/L at pH of 12.9, Fig.6c).

3.4. Quantification of Pb and sulfates phases in OPP and CAP pellets

Fig.7 gives the quantitative results of the Pb and sulfates-bearing species of OPP and CAP modelings under the studied pH ranges. At alkaline pH conditions (pH > 8), the immobilization of Pb in the OPP samples mainly relies on the adsorption and ion exchange capabilities of C-S-H and ettringite (Fig.7a). With the decrease in pH values, the neutral pH conditions are no more suitable for the equilibrium of C-S-H and ettringite. Therefore, the adsorbed Pb is gradually released as a consequence of the dissolution of hydration products. Then the soluble Pb precipitates as cerussite or is partially immobilized by the ferrihydrite ($Fe(OH)_3$) and hematite. At acidic conditions (pH <5), the Pb immobilization is attributed to the anglesite precipitation and hematite adsorption. However, non-negligible amounts of Pb remain soluble in pore solutions, as the leaching tests (Fig.6a) ascertained that the Pb leachability at pH 3.3 is a thousand times higher than the specified limit. In Fig.7b, the Pb retention of CAP samples at alkaline conditions is primarily assigned to the adsorption and ion exchange with ettringite and hematite or precipitation as $Pb(OH)_2$. At neutral pH conditions (pH 7–8), Pb leachability is dominated by hematite and ferrihydrite adsorption. Then Pb partially redissolves and reprecipitates as cerussite and anglesite, and a portion of soluble Pb remain in the pore solution in the forms of Pb^{2+}, $PbNO_3^-$, and $PbSO_{4(aq)}$ when the pH shifts to acid conditions. From Fig.7c and d, the sulfates variation of OPP and CAP samples demonstrate a similar trend in acidic conditions (pH approximately from 3 to 7). In these conditions, sulfate mainly precipitates as jarosite, anglesite, and gypsum. Whereas gypsum is the principal sulfate-bearing phase at pH values ranging from 7 to 9. The ettringite fraction increases at basic conditions, which are suitable for the stability of hydration products.

3.5. Validation of the modeling construction: mineralogical characterization of the residues

Fig.8 and S5 show the XRD quantification results from the collected OPP residues after the leaching tests at pH values of 3.3, 5.3, and 12.9 and the solid phase quantification results from the simulation. The XRD mineralogical analyses and geochemical modeling confirm the dissolution of ettringite and portlandite with decreasing pH values, whereas gypsum and jarosite are prone to precipitate at acidic conditions. However, the estimation of carbonates (calcite and vaterite) equilibrium in the modeling is less satisfactory. From the XRD quantification, carbonates are present in the OPP residues in the broad pH range studied, but the geochemical modeling indicates that the precipitation of carbonates can only be observed at highly alkaline conditions (pH 12.9, 1.2 wt%). In addition, the experimentally quantified amorphous fraction in the residues varies from 15.4 to 30.4 wt%. This observation can be better explained by the modeling results, as the amorphous fraction at basic conditions is mainly composed of C-S-H, as well as a minor content of ferrihydrite. With the acid addition, these constituents decrease gradually due to the continuous dissolution, whereas the amorphous

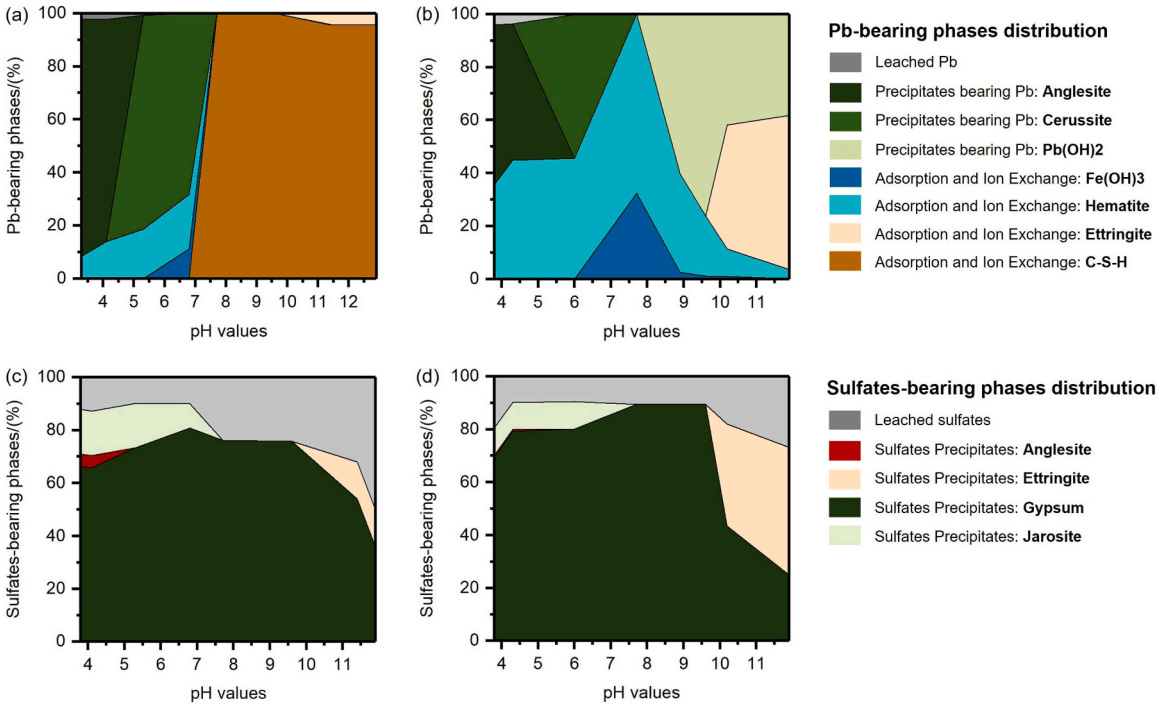

Fig. 7. The simulated PTEs-bearing phases variation as a function of pH values. (a) the variation of the Pb-bearing species in OPP samples, (b) the variation of the Pb-bearing species in CAP samples, (c) the variation of the sulfates-bearing species in OPP samples, and (d) the variation of the sulfates-bearing species in CAP samples.

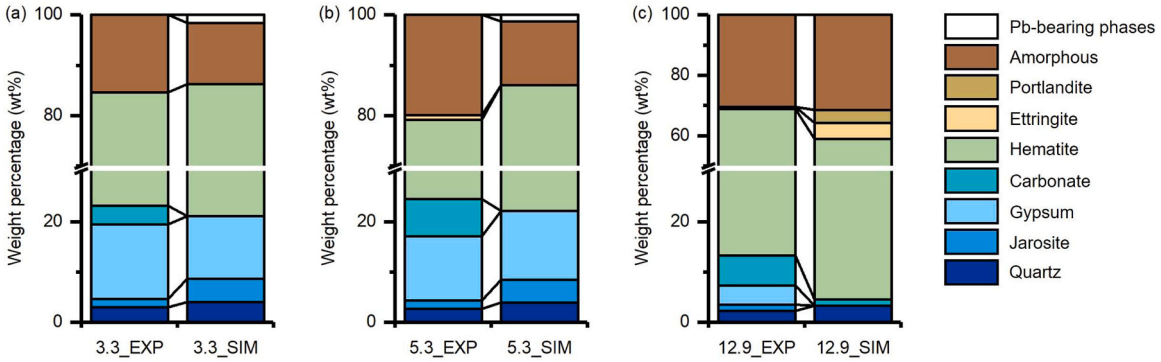

Fig. 8. The quantified mineralogical assemblages of the collected OPP residues from the XRD patterns and Phreeqc models and the correlated deviation. The leachate pH values are (a) 3.3, (b) 5.3, and (c) 12.9. The abbreviation "EXP" indicates the quantified mineralogical compositions from XRD. The abbreviation "SIM" means the quantified mineralogical compositions from modeling. The "Pb-bearing phases" is the sum of weight percentages of anglesite, cerussite, hydrocerussite, and $Pb(OH)_2$. The "amorphous" represents the experimentally quantified amorphous fraction in XRD (EXP), whereas, in simulation (SIM), it is the sum of the estimated amorphous silicates dissolved from the C-S-H matrices, amorphous C-S-H gel, amorphous $Fe(OH)_3$, and amorphous $Al(OH)_3$.

fraction is mainly assigned to amorphous silicates dissolved from the C-S-H matrices [32] and precipitated $Al(OH)_3$.

The mineralogical analyses of CAP residues performed by XRD and geochemical modeling are shown in Fig.9 and S6. Similar to the OCP characterization, the primary crystalline hydration product ettringite in CAP residues mainly precipitates in alkaline conditions. Ettringite is identified at the basic pH range (12.3 wt%, pH 11.9) and, in minor amounts, at the neutral pH range (5.1 wt%, pH 6.0). Gypsum is found in all the CAP residue samples even though the weight percentage decreases from acid to basic conditions (from 11.3 wt% to 7.0 wt%, pH from 3.8 to 11.9). In addition, the concentration of experimentally detected aluminium hydroxides (amorphous $Al(OH)_3$ and crystalline gibbsite) is in a relatively constant fraction range (22.6–24.7 wt%). The simulation also reflects this trend, but the quantified aluminium hydroxides weight percentages are only half of the experiments, with a range of 11.1–12.1 wt%. Carbonates in CAP residues are only found at the pH value of 11.9, with 1.4 and 0.9 wt% being quantified in EXP and SIM, respectively.

4. Discussion

Although the general PTEs retention mechanisms have been discussed and studied for many years [14,30,39,11], it is always challenging to quantify and clarify the exact roles of cementitious phases in PTEs immobilization. This is because the leaching of PTEs in the stabilized products is dominated by multiple physico-chemical parameters, such as the physical encapsulation from the hardened cementitious matrices [33], the dynamic changes in solid and liquid compositions [21,80], and the inherent variability of PTEs-bearing phases due to the different binder scenarios [14,81]. Traditionally, the reliability of the thermodynamic database is the major limitation in the forward geochemical modeling construction when building such a complex and dynamic process. Furthermore, leachability estimation is deficient in many case studies without fitting procedures (e.g., normalization coefficient and fraction adjustment) [16,35,45,55,6]. In the combined model presented here, adsorption and ion exchange of PTEs in multiple species from original solid waste (hematite, jarosite, and ferrihydrite) and incorporated binder phases (ettringite, C-S-H, and amorphous $Al(OH)_3$) are revealed, as well as the mechanisms of precipitation/dissolution.

In the OPP samples simulation, the retention of Pb at basic pH values is mainly controlled by the ettringite and C-S-H. In previous works without the adsorption estimation, which did not account for the effect of adsorption, the Pb stabilization at higher pH values is predominantly assigned to sparingly-soluble compound precipitations (e.g., hydrocerussite and $Pb(OH)_2$) [3,62,68]. However, the SEM results (Fig.4c) validate the Pb incorporation into the C-S-H as the Pb is concentrated along the edge of cement particles, where C-S-H commonly form by heterogeneous nucleation, with a preference for Ca and Si-enriched area. Although the Pb incorporation in ettringite is not directly observed in this work, the structural substitution of Pb in ettringite has been extensively reported [15,28,72]. This indicates that the fate of Pb in the OPP matrices is to be directly sorbed by the C-S-H, forming

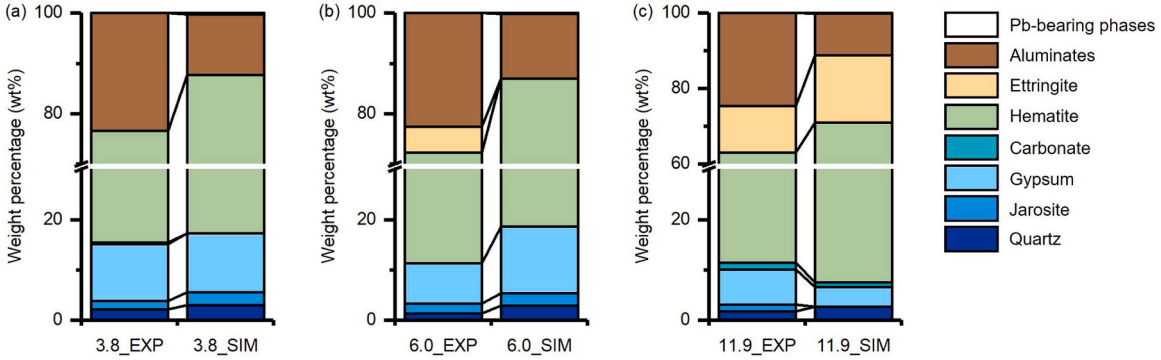

Fig. 9. The quantified mineralogical assemblages of the collected CAP residues from the XRD patterns and Phreeqc models and the correlated deviation. The leachate pH values at (a) 3.8, (b) 6.0, and (c) 11.9. The abbreviation "EXP" indicates the quantified mineralogical compositions from XRD. The abbreviation "SIM" means the quantified mineralogical compositions from modeling. The "Pb-bearing phases" is the sum of weight percentages of anglesite, cerussite, hydrocerussite, and $Pb(OH)_2$. The "aluminates" in EXP represent the experimentally quantified amorphous fraction and gibbsite in XRD, and in SIM, indicates the accumulation of amorphous $Al(OH)_3$ and crystalline gibbsite.

Pb-enriched outer rings distributed around the cement particles [72]. The increase in pH values of the environment (from 10.9 to 12.9) is well-known to slightly affect the solubility of hydration products. Therefore, under such conditions, the Pb would likely form hydroxides and be preserved in an alkaline environment according to the widely reported hypothesis of hydroxide precipitation [64,65,71]. With the pH values moving to neutral conditions, the model (Fig.7a) indicates that the minimum of the Pb leaching curve (Fig.6a) is dominated by precipitation of anglesite and cerussite and adsorption by hematite and ferrihydrite. However, other studies suggested that the enhanced Pb immobilization is mainly related to the encapsulation from the hardened cementitious phases, which efficiently prevents Pb leaching [2,33,51,62]. Therefore, to give a better representation of Pb leachability, Solpuker et al., [62] estimated that only 10% of the phases would take part in the dissolution/precipitation process when the pH values of the system are lower than 11. Similar specific leaching coefficients of 31% and 40% are also introduced in the work of Halim et al., [33] and Berthomier et al., [2], respectively. The Pb speciation of simulated OPP samples under acidic conditions (pH<5, Fig.7a) confirms the results of previous investigations [13,14] that anglesite precipitation is the primary Pb-bearing phase in this equilibrium. Consequently, due to the high acidity of the system, a considerable amount of soluble Pb is released into the solution.

Regarding the Pb immobilization in CAP samples at basic conditions (Fig.7b), it is not surprising that ettringite is the main contributor, with approximately 58% of Pb stabilized by ettringite which is approximately ten times higher than the relative percentage in OPP samples (4%, pH 12.9). In addition, although the adsorption by means of amorphous Al$(OH)_3$ is defined in the CAP modeling system (Table.S2), 38% of Pb is stabilized by the precipitation of $Pb(OH)_2$ at the pH value of 11.9, unlike the OPP systems, where most of the Pb available is incorporated in C-S-H (Fig.7a). This difference is possibly assigned to the relatively low Pb concentrations in both systems, as the Pb fraction is lower than 1 wt%. When the concentration of Pb exceeds the amount that can be bound to the surfaces of host phases, the excess Pb forms hydroxides. Therefore, in the OPP system, the high specific surface area and the layered structure of C-S-H may maximize the Pb adsorption capacity. Wang and Wang [72] reported a similar finding, as they observed that adsorption onto C-S-H and Pb hydroxide precipitation plays an approximately equivalent role in Pb immobilization. By contrast, in the CAP system, the specific surface area of amorphous Al$(OH)_3$ is much lower compared to C-S-H (Table.S2), giving the overall system a relatively low sorption capacity compared to the OPP samples. Therefore, in this system, Pb immobilization is mostly controlled by ettringite and precipitation of hydroxides. Another interesting difference is that when the pH values are slightly acidic (pH from 4 to 7), Pb in CAP dissolved from the ferrihydrite surface and partially precipitated as cerussite and anglesite. However, the relative Pb fraction captured by hematite is nearly constant at 45% (Fig.7d), which ascertains the assumption of overall system maximum adsorption capacity. Because of the physical encapsulation defined in this work, the total amount of Pb input within CAP samples is estimated to be only a quarter of OPP samples (Table.S2). Therefore, after all the active binding sites of hematite are occupied by Pb, the remaining soluble Pb reacts with the sulfates dissolved from the ettringite and slightly dissolved CO_2 from the atmosphere. Since the amount of Pb defined in OPP samples is higher than in CAP, more soluble Pb would be released to the pore solution and induce the precipitation of additional Pb-bearing phases. Consequently, different Pb retention mechanisms were shown.

To further quantify the relative Pb host capacities (ion exchange, adsorption, and precipitation) of the phases defined in the model, excluding the effects of estimated physical encapsulation, we calculated the relative capacity of each phase in the studied pH range (Fig.10). The results reveal that the cementitious matrices (ettringite and C-S-H) have greater Pb capacities compared to the phases present in PA samples (hematite, jarosite, and ferrihydrite). Obviously, the enhanced Pb capacity of cementitious matrices is more efficient at high pH conditions due to their inherent stability at such pH values (Fig.10a and b). When the cementitious matrices cannot effectively stabilize all the soluble Pb in the system, hematite and ferrihydrite contribute to its uptake (Fig.10c and d). Similar experimental findings were also reported in the literature

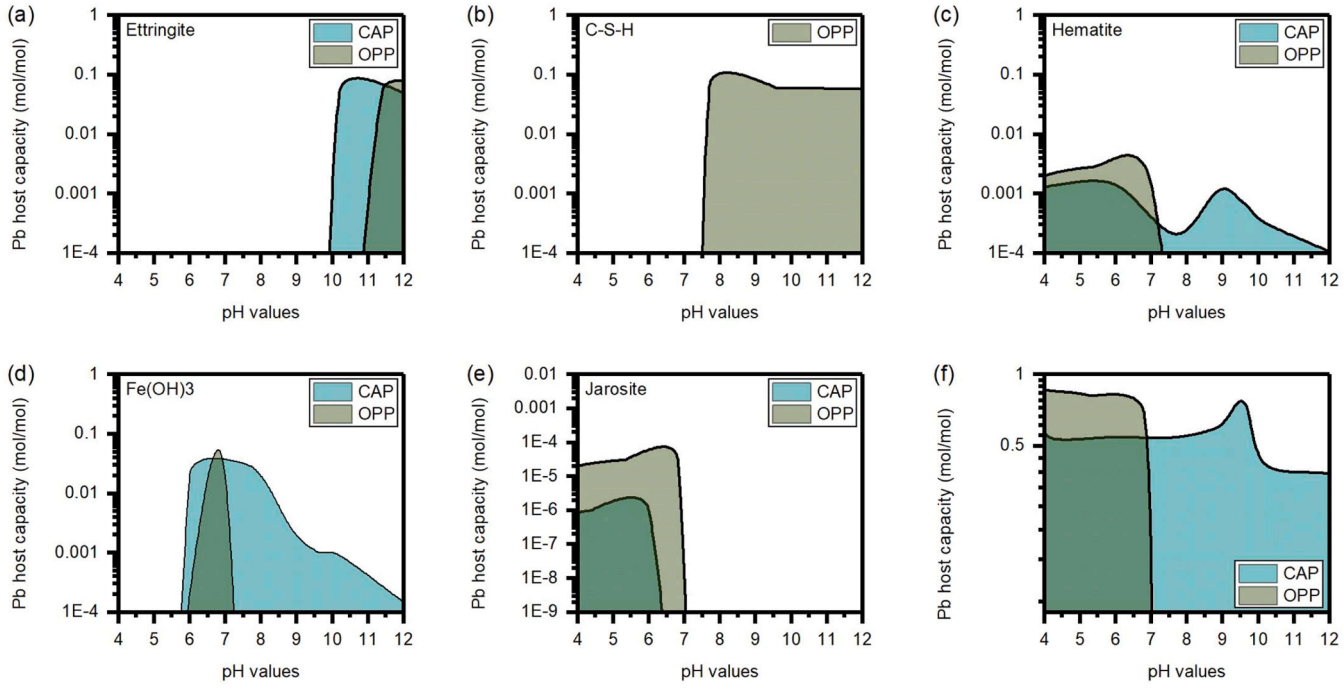

Fig. 10. The relative Pb hosting capacities of multiple phases in OPP and CAP (mol/mol). (a) ettringite, (b) C-S-H, only present in OPP samples, (c) hematite, (d) Fe$(OH)_3$, (e) jarosite, and (f) Pb-precipitations. Note that the Pb host capacities with adsorption and ion exchange are calculated by dividing the mole content of adsorbed Pb by the mole content of attributed phases. (e.g., 1 mol of Pb is adsorbed by 10 mol C-S-H, then the Pb host capacity is 0.1 mol/mol). The Pb host capacity in image f indicates the mole percentage of anglesite, cerussite, and $Pb(OH)_2$ with respect to the immobilized Pb.

[49,71]. In fact, without solidification/stabilization, the Pb incorporation into the iron (oxyhydr)oxides takes place between neutral and alkaline pH. Moreover, Pb can only be released from the iron phases at highly acidic conditions (pH <2) or during reductive dissolution (e.g., if the colloids are buried within anaerobic sediments) [49,71].

Interestingly, although the current simulation conforms to the experimental Pb leaching profile (Fig.6a and b) and the variation of mineralogical composition (Figs. 8 and 9), there are some limitations to our interpretation, i.e., the estimation of carbonates and sulfates dissolution/precipitation in this pH range needs to be further investigated and optimized. The overestimation of carbonates could be partially attributed to the kinetic of calcite dissolution. Although the pH decrease is one of the critical factors controlling the dissolution of the carbonates, both the porosity of the samples and the concentration gradient in the local aqueous phase conditions can also be essential mechanisms when applied in natural systems, as a previous investigation indicates that the calcite fluctuates between precipitation and dissolution [52]. With respect to the sulfate leaching, the estimation in both CAP and OPP profiles under acidic conditions is relatively acceptable. However, the sulfate release from the OPP samples under alkaline conditions differed from the experimental results, with an upward increase in the simulated leaching curve, while this increase was not observed in the experimental results (Fig.6c). One possible explanation for this leaching deviation is that the model ideally calculates chemical equilibria and does not reflect the reaction kinetics (e.g., dissolution/precipitation kinetics) and physical information (e.g., changes in porosity). The sulfate concentration of OPP and CAP samples under alkaline conditions is dominated by ettringite, gypsum, and aluminate balance. At highly alkaline conditions (pH>10), which enable the ettringite precipitation, the dissolution of gypsum is herein increased in order to provide additional sulfate for the formation of ettringite, thus compensating for the sulfate scarcity. However, in real cases, ettringite formation and dissolution is also a kinetically controlled process [77], which was not considered in the modeling of this work. As a result, at high pH values (Figs.8c and 9c), ettringite is oversaturated in both the OPP and CAP systems, and therefore its weight fraction is overestimated. Accordingly, the weight fractions of gypsum and aluminates from the PHREEQC simulation are underestimated. In order to interpret a reliable description of this kinetic process, a reactive transport model involving rate constant, diffusion coefficient, and surface complexation constant can be implemented in future works. Furthermore, it is worth noting that in OPP samples more calcite is observed in experimental quantification results (Fig.8), which could be partially related to the extra carbonation during air-drying. As this procedure may lead to the accelerated carbonation of ettringite and amorphous content (mainly C-S-H) in OPC-based mixtures [34].

In general, our developed method enables a better understanding of the PTEs immobilization roles of the main hydration products and inherent phases in solid waste, which is hardly revealed by the experimental techniques. In turn, understanding the extent of this role variation will allow a more accurate and reliable mixture design for the in-situ remediation industry. The implications of these results underscore the importance of not only predicting and clarifying the PTEs immobilization amounts as a function of pH values but also highlighting the essential question of how the stabilized products would contribute to PTEs retention when the field conditions are under harsh or unsuitable conditions. For example, when the pH of the rainfall and groundwater changes with the season or anthropogenic activities, the predicted concentrations of dissolved PTEs could be used to forecast whether secondary pollution will occur.

Ultimately, we stress that our approach has certain limitations, as its input data depends on a relatively comprehensive mineralogical and chemical characterization of the samples. This is due to the inherent nature of cement hydration systems, which contain a large number of amorphous hydration products (Fig.3, e.g., C-S-H in OPP and CAH in CAP). Quantifying the mass fraction of these amorphous contents in the stabilized products is necessary for our model, not only because they are important hosts for PTEs that can be retained by means of chemical stabilization, but they also provide considerable physical encapsulation to the overall systems to prevent the PTEs from getting contact with the leachate. Future work could therefore aim to develop a 'cradle to gate' model for the S/S process, using the bulk characterization of raw waste and binder as model inputs to predict the composition of the waster-binder mixtures as well as the leaching behavior of the PTEs. In addition, we recognize that the reliability and accuracy of our present model can be improved by further efforts of data collection in PTEs pH-dependent leachability with different PTEs concentrations and different mixtures proportions. Should the changes be significant, the model will need to be re-assessed and re-calibrated.

5. Conclusion

This study explores the role of the PTEs immobilization capacity of cementitious phases and solid wastes phases in a broad pH range. The Pb-rich PA waste was stabilized in traditional (OPC) and alternative (CAC) binders to optimize the Pb leachability and mitigate CO_2 emissions. The experimental and modeling investigations contribute to the understanding of the solidification/stabilization mechanisms of each scenario. The following conclusions can be drawn based on the results obtained from the experiment and modeling:

(1) both scenarios demonstrate high retention of Pb at neutral and alkaline pH conditions (approximately from 7 to 11). The use of CAC binder effectively enhanced the Pb retention capacity of the stabilized products, especially in harsh acid conditions, with only a quarter of Pb concentration detected in CAP samples (11000 μg/L) compared to OPP samples (43000 μg/L). Experiments reveal that Pb incorporation in OPP samples is mainly associated with the presence of C-S-H, with an observed enrichment in Ca and Si-rich areas along the cement particles (where C-S-H precipitation occurs), whereas the Pb is homogeneously distributed in the CAP samples.

(2) Geochemical modeling reveals that C-S-H adsorption is the primary Pb immobilization mechanism of OPP samples under alkaline conditions, with a 0.1 mol/mol Pb retention capacity that can be reached. When the pH is unsuitable for C-S-H precipitation, cerussite and anglesite precipitation are the main controls of Pb leachability, with small amounts of soluble Pb being adsorbed by hematite and ferrihydrite.

(3) Regarding the CAP samples, precipitation of $Pb(OH)_2$ and incorporation in ettringite are the primary control mechanisms for Pb equilibrium in alkaline environments. The Pb host capacity of ettringite is estimated to be approximately 0.1 mol/mol, which is equivalent to C-S-H. However, the contribution of hematite and ferrihydrite adsorption to Pb equilibrium is observed in a broader pH range compared to OPP samples. Likewise, the cerussite and anglesite precipitation shows stronger affinities for Pb immobilization in acid conditions.

(4) The sulfate release in both cases is at a steady state, varying from 600 to 900 mg/L in all experiments conducted. The modeling results suggest that sulfate retention is controlled by the dissolution and precipitation of anglesite, gypsum, ettringite, and jarosite. But the estimation of sulfate leachability is relatively limited, particularly in the OPP samples, which might be influenced by the equilibrium kinetics of ettringite. Further work is in progress to assess the impact of the dissolution/precipitation kinetics of the discussed phases for PTEs immobilization.

Environmental implications

Potentially toxic elements (PTEs) pollution from industrial activities have driven land degradation with detrimental to human health. In-situ remediation has been proven to be important for the sustainable management of brownfield sites, but there is a limited empirical analysis of the underlying mechanisms responsible for PTEs leaching. This study proposed an integrated framework that employs the geochemical model

PHREEQC and parameter-fitting software PEST+ + to clarify and quantify the impacts of multiple physicochemical constituents (e.g., physical encapsulation, ion exchange, adsorption, precipitation, and dissolution) in controlling PTEs retention across a wide pH range, which is challenging to be revealed by experiments.

CRediT authorship contribution statement

Yikai Liu: Conceptualization, Writing – original draft, Investigation, Formal analysis. **Simone Molinari:** Conceptualization, Validation, Writing – review & editing, Investigation, Visualization. **Maria Chiara Dalconi:** Validation, Investigation, Visualization, Writing – review & editing. **Luca Valentini:** Investigation, Validation, Visualization, Writing – review & editing. **Maurizio Pietro Bellotto:** Resources, Investigation. **Giorgio Ferrari:** Resources, Supervision. **Roberto Pellay:** Resources, Investigation. **Graziano Rilievo:** Writing – review & editing. **Fabio Vianello:** Investigation, Writing – review & editing. **Gabriella Salviulo:** Validation, Investigation. **Qiusong Chen:** Resources, Validation. **Gilberto Artioli:** Conceptualization, Writing – review & editing, Project administration, Resources, Supervision, Validation. All the authors discussed the data and agreed on their interpretations. All the co-authors contributed to the final polishing of the manuscript.

Declaration of Competing Interest

The authors declare that they have no known competing financial interests or personal relationships that could have appeared to influence the work reported in this paper.

Data Availability

Data will be made available on request.

Acknowledgments

This research was funded by the National Natural Science Foundation of China (No. 552104156, 52074351, and 52004330), the Science and Technology Innovation Program of Hunan Province (No. 2021RC3125), a scholarship granted by the China Scholarship Council (No.CSC201906370062), and the PRIN project "Mineral reactivity, a key to understand large-scale processes: from rock-forming environments to solid waste recovering/lithification" n. 2017L83S77. The author would like to thank Dr. Daria Pasqual (University of Padua) for the XRF analyses and acknowledge the valuable advice provided by Dr. C.A.J. Appelo (Hydrochemical Consultant Amsterdam).

Appendix A. Supporting information

Supplementary data associated with this article can be found in the online version at doi:10.1016/j.jhazmat.2023.131849.

References

[1] Appelo, C.A.J., Parkhurst, D.L., Post, V.E.A., 2014. Equations for calculating hydrogeochemical reactions of minerals and gases such as CO_2 at high pressures and temperatures. Geochim Et Cosmochim Acta v. 125, 49–67. https://doi.org/10.1016/J.GCA.2013.10.003.

[2] Berthomier, M., Lors, C., Damidot, D., De Larrard, T., Guérandel, C., Bertron, A., 2021. Leaching of CEM III paste by demineralised or mineralised water at pH 7 in relation with aluminium release in drinking water network. Cem Concr Res v. 143. https://doi.org/10.1016/J.CEMCONRES.2021.106399.

[3] Bobirică, C., Long, D.T., Parsons, M.J., Stănescu, R., Voice, T.C., 2018. Examination of the influence of dissolved halite (NaCl) on the leaching of lead (Pb) from cement-based solidified wastes. J Mater Cycles Waste Manag v. 20, 59–70. https://doi.org/10.1007/S10163-016-0552-6/FIGURES/8.

[4] Bonomo, L., Careghini, A., Dastoli, S., De Propris, L., Ferrari, G., Gabellini, M., et al., 2009. Feasibility studies for the treatment and reuse of contaminated marine sediments. Environ. Technol. v. 30, 817–823. https://doi.org/10.1080/09593330902990105. ⟨https://doi.org/10.1080/09593330902990105⟩.

[5] Calgaro, L., Contessi, S., Bonetto, A., Badetti, E., Ferrari, G., Artioli, G., et al., 2021. Calcium aluminate cement as an alternative to ordinary Portland cement for the remediation of heavy metals contaminated soil: mechanisms and performance. J Soils Sediment. https://doi.org/10.1007/s11368-020-02859-x.

[6] Chen, J., Fu, C., Mao, T., Shen, Y., Li, M., Lin, X., et al., 2022. Study on the accelerated carbonation of MSWI fly ash under ultrasonic excitation: CO_2 capture, heavy metals solidification, mechanism and geochemical modelling. Chem Eng J v. 450, 138418. https://doi.org/10.1016/J.CEJ.2022.138418.

[7] Chen, K., Jin, X., Guo, C., He, C., Zhang, Y., Gao, K., et al., 2021. Reductive dissolution of Pb-Zn jarosite under near-neutral conditions. Chem Geol v. 579, 120338. https://doi.org/10.1016/J.CHEMGEO.2021.120338.

[8] Chen, L., Wang, Y.S., Wang, L., Zhang, Y., Li, J., Tong, L., et al., 2021. Stabilisation/solidification of municipal solid waste incineration fly ash by phosphate-enhanced calcium aluminate cement. J Hazard Mater v. 408, 124404. https://doi.org/10.1016/J.JHAZMAT.2020.124404.

[9] Chen, L., Wang, L., Zhang, Y., Ruan, S., Mechtcherine, V., Tsang, D.C.W., 2022. Roles of biochar in cement-based stabilization/solidification of municipal solid waste incineration fly ash. Chem Eng J v. 430, 132972. https://doi.org/10.1016/J.CEJ.2021.132972.

[10] Chen, L., Zhang, Y., Wang, L., Ruan, S., Chen, J., Li, H., et al., 2022. Biochar-augmented carbon-negative concrete. Chem Eng J v. 431, 133946. https://doi.org/10.1016/j.cej.2021.133946.

[11] Chen, Q.Y., Tyrer, M., Hills, C.D., Yang, X.M., Carey, P., 2009. Immobilisation of heavy metal in cement-based solidification/stabilisation: a review. Waste Manag. https://doi.org/10.1016/j.wasman.2008.01.019.

[12] Chen, Z., Zhang, P., Brown, K.G., Branch, J.L., van der Sloot, H.A., Meeussen, J.C. L., et al., 2021. Development of a geochemical speciation model for use in evaluating leaching from a cementitious radioactive waste form. Environ Sci Technol v. 55, 8642–8653. https://doi.org/10.1021/ACS.EST.0C06227/ASSET/IMAGES/LARGE/ES0C06227_0007.JPEG.

[13] Chukwura, U.O., Hursthouse, A.S., 2020. Evaluating controls on potentially toxic element release in circum-neutral mine water: a case study from the abandoned Pb–Zn mines of Leadhills and Wanlockhead, South of Scotland. U Kingd: Environ Earth Sci v. 79, 1–13. https://doi.org/10.1007/S12665-020-09108-X/FIGURES/5.

[14] Contessi, S., Calgaro, L., Dalconi, M.C., Bonetto, A., Bellotto, M., Pietro, et al., 2020. Stabilization of lead contaminated soil with traditional and alternative binders. J Hazard Mater. https://doi.org/10.1016/j.jhazmat.2019.120990.

[15] Contessi, S., Dalconi, M.C., Pollastri, S., Calgaro, L., Meneghini, C., Ferrari, G., et al., 2021. Cement-stabilized contaminated soil: understanding Pb retention with XANES and Raman spectroscopy. Sci Total Environ v. 752, 141826. https://doi.org/10.1016/J.SCITOTENV.2020.141826.

[16] Cornelis, G., Etschmann, B., Van Gerven, T., Vandecasteele, C., 2012. Mechanisms and modelling of antimonate leaching in hydrated cement paste suspensions. Cem Concr Res v. 42, 1307–1316. https://doi.org/10.1016/J.CEMCONRES.2012.06.004.

[17] Damion, T., Chaunsali, P., 2022. Evaluating acid resistance of Portland cement, calcium aluminate cement, and calcium sulfoaluminate based cement using acid neutralisation. Cem Concr Res v. 162, 107000. https://doi.org/10.1016/J.CEMCONRES.2022.107000.

[18] De Kleijne, K., Hanssen, S.V., Van Dinteren, L., Huijbregts, M.A.J., Van Zelm, R., De Coninck, H., 2022. Limits to Paris compatibility of CO 2 capture and utilization. One Earth v. 5, 168–185. https://doi.org/10.1016/j.oneear.2022.01.006.

[19] Deng, H., Tian, C., Li, L., Liang, Y., Yan, S., Hu, M., et al., 2022. Microinteraction analysis between heavy metals and coexisting phases in heavy metal containing solid wastes. ACS EST Eng v. 2, 547–563. https://doi.org/10.1021/ACSESTENGG.1C00343.

[20] Dijkstra, J.J., Van der Sloot, H.A., Comans, R.N.J., 2002. Process identification and model development of contaminant transport in MSWI bottom ash. Waste Manag v. 22, 531–541. https://doi.org/10.1016/S0956-053X(01)00034-4.

[21] Dijkstra, J.J., Van Der Sloot, H.A., Comans, R.N.J., 2006. The leaching of major and trace elements from MSWI bottom ash as a function of pH and time. Appl Geochem v. 21, 335–351. https://doi.org/10.1016/J.APGEOCHEM.2005.11.003.

[22] Doherty, J., 2015, Calibration and Uncertainty Analysis for Complex Environmental Models PEST: complete theory and what it means for modelling the real world:, www.pesthomepage.org (accessed August 2022).

[23] Du, B., Li, J., Fang, W., Liu, J., 2019. Comparison of long-term stability under natural ageing between cement solidified and chelator-stabilised MSWI fly ash. Environ Pollut v. 250, 68–78. https://doi.org/10.1016/J.ENVPOL.2019.03.124.

[24] Dzombak, D.A., and Morel, F.M.M., 1990, Surface Complexation Modeling: Hydrous Ferric Oxide. A Wiley-Interscience publication (J. W. & Sons, Ed.):, p. 393, https://www.wiley.com/en-us/Surface+Complexation+Modeling%3A+Hydrous+Ferric+Oxide-p-9780471637318 (accessed February 2023).

[25] Forray, F.L., Smith, A.M.L., Drouet, C., Navrotsky, A., Wright, K., Hudson-Edwards, K.A., et al., 2010. Synthesis, characterization and thermochemistry of a Pb-jarosite. Geochim Et Cosmochim Acta v. 74, 215–224. https://doi.org/10.1016/J.GCA.2009.09.033.

[26] Frau, F., Ardau, C., Fanfani, L., 2009. Environmental geochemistry and mineralogy of lead at the old mine area of Baccu Locci (south-east Sardinia, Italy). J Geochem Explor v. 100, 105–115. https://doi.org/10.1016/J.GEXPLO.2008.01.005.

[27] Gabarrón, M., Babur, O., Soriano-Disla, J.M., Faz, A., Acosta, J.A., 2018. Composition and risk assessment of roasted pyrite ash from fertiliser production. Chemosphere v. 209, 277–285. https://doi.org/10.1016/J.CHEMOSPHERE.2018.06.109.

[28] Gougar, M.L.D., Scheetz, B.E., Roy, D.M., 1996. Ettringite and C□S□H Portland cement phases for waste ion immobilization: a review. Waste Manag v. 16, 295–303. https://doi.org/10.1016/S0956-053X(96)00072-4.
[29] Gualtieri, A.F., 2000. Accuracy of XRPD QPA using the combined Rietveld–RIR method. urn:issn:0021-8898 v. 33, 267–278. https://doi.org/10.1107/S002188989901643X.
[30] Guo, B., Liu, B., Yang, J., Zhang, S., 2017. The mechanisms of heavy metal immobilization by cementitious material treatments and thermal treatments: a review. J Environ Manag v. 193, 410–422. https://doi.org/10.1016/j.jenvman.2017.02.026.
[31] Guo, B., Tan, Y., Wang, L., Chen, L., Wu, Z., Sasaki, K., et al., 2021. High-efficiency and low-carbon remediation of zinc contaminated sludge by magnesium oxysulfate cement. J Hazard Mater v. 408, 124486. https://doi.org/10.1016/J.JHAZMAT.2020.124486.
[32] Gutberlet, T., Hilbig, H., Beddoe, R.E., 2015. Acid attack on hydrated cement - effect of mineral acids on the degradation process. Cem Concr Res. https://doi.org/10.1016/j.cemconres.2015.03.011.
[33] Halim, C.E., Short, S.A., Scott, J.A., Amal, R., Low, G., 2005. Modelling the leaching of Pb, Cd, As, and Cr from cementitious waste using PHREEQC. J Hazard Mater v. 125, 45–61. https://doi.org/10.1016/j.jhazmat.2005.05.046.
[34] Hames, B., Ruiz, R., Scarlata, C., Sluiter, A., Sluiter, J., Templeton, D., 2008. Preparation of samples for compositional analysis. Lab Anal Proced (LAP). Issue Date 08/08/2008.
[35] Helser, J., Cappuyns, V., 2021. Trace elements leaching from PbZn mine waste (Plombières, Belgium) and environmental implications. J Geochem Explor v. 220, 106659. https://doi.org/10.1016/J.GEXPLO.2020.106659.
[36] Helser, J., Cappuyns, V., 2022. Acid generation potential and kinetics of metal (loid) release from resuspended sulfidic mine waste. J Environ Chem Eng v. 10, 108158. https://doi.org/10.1016/J.JECE.2022.108158.
[37] Hoeber, L., Steinlechner, S., 2021. A comprehensive review of processing strategies for iron precipitation residues from zinc hydrometallurgy. Clean Eng Technol v. 4, 100214. https://doi.org/10.1016/J.CLET.2021.100214.
[38] Holmes, N., Tyrer, M., West, R., Lowe, A., Kelliher, D., 2022. Using PHREEQC to model cement hydration. Constr Build Mater v. 319, 126129. https://doi.org/10.1016/J.CONBUILDMAT.2021.126129.
[39] Hossain, M.U., Wang, L., Chen, L., Tsang, D.C.W., Ng, S.T., Poon, C.S., et al., 2020. Evaluating the environmental impacts of stabilization and solidification technologies for managing hazardous wastes through life cycle assessment: a case study of Hong Kong. Environ Int v. 145, 106139. https://doi.org/10.1016/J.ENVINT.2020.106139.
[40] Hou, D., O'Connor, D., Igalavithana, A.D., Alessi, D.S., Luo, J., Tsang, D.C.W., et al., 2020. Metal contamination and bioremediation of agricultural soils for food safety and sustainability. Nat Rev Earth Environ v. 1, 366–381. https://doi.org/10.1038/s43017-020-0061-y.
[41] Jarošíková, A., Ettler, V., Mihaljevič, M., Drahota, P., Culka, A., Racek, M., 2018. Characterization and pH-dependent environmental stability of arsenic trioxide-containing copper smelter flue dust. J Environ Manag v. 209, 71–80. https://doi.org/10.1016/J.JENVMAN.2017.12.044.
[42] Klaus, S.R., Neubauer, J., Goetz-Neunhoeffer, F., 2013. Hydration kinetics of CA2 and CA—investigations performed on a synthetic calcium aluminate cement. Cem Concr Res v. 43, 62–69. https://doi.org/10.1016/J.CEMCONRES.2012.09.005.
[43] Kumpiene, J., Antelo, J., Brännvall, E., Carabante, I., Ek, K., Komárek, M., et al., 2019. In situ chemical stabilization of trace element-contaminated soil – field demonstrations and barriers to transition from laboratory to the field – a review. Appl Geochem v. 100, 335–351. https://doi.org/10.1016/J.APGEOCHEM.2018.12.003.
[44] Liu, S., Cui, S., Guo, H., Wang, Y., Zheng, Y., 2021. Adsorption of lead ion from wastewater using non-crystal hydrated calcium silicate gel. v. 14, p. 842 Materials Vol. 14, 842. https://doi.org/10.3390/MA14040842.
[45] Liu, Y., Chen, Q., Dalconi, M.C., Molinari, S., Valentini, L., Wang, Y., et al., 2022. Retention of phosphorus and fluorine in phosphogypsum for cemented paste backfill: experimental and numerical simulation studies. Environ Res, 113775. https://doi.org/10.1016/J.ENVRES.2022.113775.
[46] Liu, Y., Molinari, S., Dalconi, M.C., Valentini, L., Ricci, G., Carrer, C., et al., 2023. The leaching behaviors of lead, zinc, and sulfate in pyrite ash contaminated soil: mineralogical assessments and environmental implications. J Environ Chem Eng v. 11, 109687. https://doi.org/10.1016/J.JECE.2023.109687.
[47] Lothenbach, B., Kulik, D.A., Matschei, T., Balonis, M., Baquerizo, L., Dilnesa, B., et al., 2019. Cemdata18: a chemical thermodynamic database for hydrated Portland cements and alkali-activated materials. Cem Concr Res. https://doi.org/10.1016/j.cemconres.2018.04.018.
[48] Lu, P., Zhang, G., Apps, J., Zhu, C., 2022. Comparison of thermodynamic data files for PHREEQC. Earth-Sci Rev v. 225, 103888. https://doi.org/10.1016/J.EARSCIREV.2021.103888.
[49] Lu, Y., Hu, S., Liang, Z., Zhu, M., Wang, Z., Wang, X., et al., 2020. Incorporation of Pb(ii) into hematite during ferrihydrite transformation. Environ Sci: Nano v. 7, 829–841. https://doi.org/10.1039/C9EN01355E.
[50] Malviya, R., Chaudhary, R., 2006. Factors affecting hazardous waste solidification/stabilization: a review. J Hazard Mater v. 137, 267–276. https://doi.org/10.1016/J.JHAZMAT.2006.01.065.
[51] Martens, E., Jacques, D., Van Gerven, T., Wang, L., Mallants, D., 2010. Geochemical modeling of leaching of Ca, Mg, Al, and Pb from cementitious waste forms. Cem Concr Res v. 40, 1298–1305. https://doi.org/10.1016/J.CEMCONRES.2010.01.007.
[52] Matteo, E.N., Huet, B., Jové-Colón, C.F., Scherer, G.W., 2018. Experimental and modeling study of calcium carbonate precipitation and its effects on the degradation of oil well cement during carbonated brine exposure. Cem Concr Res v. 113, 1–12. https://doi.org/10.1016/J.CEMCONRES.2018.03.016.
[53] Oliveira, M.L.S., Ward, C.R., Izquierdo, M., Sampaio, C.H., de Brum, I.A.S., Kautzmann, R.M., et al., 2012. Chemical composition and minerals in pyrite ash of an abandoned sulphuric acid production plant. Sci Total Environ v. 430, 34–47. https://doi.org/10.1016/J.SCITOTENV.2012.04.046.
[54] Ouhadi, V.R., Yong, R.N., Deiranlou, M., 2021. Enhancement of cement-based solidification/stabilization of a lead-contaminated smectite clay. J Hazard Mater v. 403, 123969. https://doi.org/10.1016/J.JHAZMAT.2020.123969.
[55] Pang, L., Wang, D., Wang, H., An, M., Wang, Q., 2022. Occurrence and leaching behaviors of heavy-metal elements in metallurgical slags. Constr Build Mater v. 330, 127268. https://doi.org/10.1016/J.CONBUILDMAT.2022.127268.
[56] Parbhakar-Fox, A., 2016. Geoenvironmental characterisation of heap leach materials at abandoned mines: croydon Au-mines, QLD, Australia. v. 6, p. 52 Minerals Vol. 6, 52. https://doi.org/10.3390/MIN6020052.
[57] Parkhurst, D.L., and Appelo, C.A.J., 2013, Description of Input and Examples for PHREEQC Version 3 — A Computer Program for Speciation, Batch-Reaction, One-Dimensional Transport, and Inverse Geochemical Calculations.: U.S. Geological Survey Techniques and Methods, book 6, chapter A43,.
[58] Puppala, A.J., Talluri, N., Congress, S.S.C., Gaily, A., 2018. Ettringite induced heaving in stabilized high sulfate soils. Innov Infrastruct Solut v. 3, 1–12. https://doi.org/10.1007/S41062-018-0179-7/FIGURES/10.
[59] Qoku, E., Bier, T.A., Schmidt, G., Skibsted, J., 2022. Impact of sulphate source on the hydration of ternary pastes of Portland cement, calcium aluminate cement and calcium sulphate. Cem Concr Compos v. 131, 104502. https://doi.org/10.1016/J.CEMCONCOMP.2022.104502.
[60] Rietveld, H.M., 1969. A profile refinement method for nuclear and magnetic structures. J Appl Crystallogr v. 2, 65–71. https://doi.org/10.1107/S0021889869006558.
[61] Shi, M., Min, X., Tian, C., Hao, T., Zhu, S., Ge, Y., et al., 2022. Mechanisms of Pb(II) coprecipitation with natrojarosite and its behavior during acid dissolution. J Environ Sci v. 122, 128–137. https://doi.org/10.1016/J.JES.2021.10.006.
[62] Solpuker, U., Sheets, J., Kim, Y., Schwartz, F.W., 2014. Leaching potential of pervious concrete and immobilization of Cu, Pb and Zn using pervious concrete. J Contam Hydrol. https://doi.org/10.1016/j.jconhyd.2014.03.002.
[63] Steiner, S., Lothenbach, B., Proske, T., Borgschulte, A., Winnefeld, F., 2020. Effect of relative humidity on the carbonation rate of portlandite, calcium silicate hydrates and ettringite. Cem Concr Res v. 135, 106116. https://doi.org/10.1016/J.CEMCONRES.2020.106116.
[64] Štulović, M., Radovanović, D., Kamberović, Ž., Korać, M., Anđić, Z., 2019. Assessment of leaching characteristics of solidified products containing secondary alkaline lead slag. v. 16, p. 2005 Int J Environ Res Public Health 2019 Vol. 16, 2005. https://doi.org/10.3390/IJERPH16112005.
[65] Sun, J., Wang, L., Yu, J., Guo, B., Chen, L., Zhang, Y., et al., 2022. Cytotoxicity of stabilized/solidified municipal solid waste incineration fly ash. J Hazard Mater v. 424, 127369. https://doi.org/10.1016/J.JHAZMAT.2021.127369.
[66] Sun, Z., Vollpracht, A., van der Sloot, H.A., 2019. pH dependent leaching characterization of major and trace elements from fly ash and metakaolin geopolymers. Cem Concr Res v. 125, 105889. https://doi.org/10.1016/J.CEMCONRES.2019.105889.
[67] Tang, W., Guo, B., Li, Z., Zhao, X., Gu, X., 2022. Flooding and drainage induced abiotic reactions control metal solubility in soil of a contaminated industrial site. Chemosphere v. 297, 134032. https://doi.org/10.1016/J.CHEMOSPHERE.2022.134032.
[68] Tangviroon, P., et al., 2020. Immobilization of lead and zinc leached from mining residual materials in kabwe, zambia: possibility of chemical immobilization by dolomite, calcined dolomite, and magnesium oxide. v. 10, p. 763 Minerals 2020 Vol. 10, 763. https://doi.org/10.3390/MIN10090763.
[69] Torres-Martínez, J.A., Mora, A., Knappett, P.S.K., Ornelas-Soto, N., Mahlknecht, J., 2020. Tracking nitrate and sulfate sources in groundwater of an urbanized valley using a multi-tracer approach combined with a Bayesian isotope mixing model. Water Res v. 182, 115962. https://doi.org/10.1016/J.WATRES.2020.115962.
[70] Vega-Garcia, P., Schwerd, R., Schwitalla, C., Johann, S., Scherer, C., Helmreich, B., 2021. Leaching prediction for vertical test panels coated with plaster and mortars exposed under real conditions by a PHREEQC leaching model. Chemosphere v. 280, 130657. https://doi.org/10.1016/J.CHEMOSPHERE.2021.130657.
[71] Vu, H.P., Shaw, S., Brinza, L., Benning, L.G., 2013. Partitioning of Pb(II) during goethite and hematite crystallization: Implications for Pb transport in natural systems. Appl Geochem v. 39, 119–128. https://doi.org/10.1016/J.APGEOCHEM.2013.10.001.
[72] Wang, D., Wang, Q., 2022. Clarifying and quantifying the immobilization capacity of cement pastes on heavy metals. Cem Concr Res v. 161, 106945. https://doi.org/10.1016/J.CEMCONRES.2022.106945.
[73] Wang, H., Ju, C., Zhou, M., Chen, J., Dong, Y., Hou, H., 2022. Sustainable and efficient stabilization/solidification of Pb, Cr, and Cd in lead-zinc tailings by using highly reactive pozzolanic solid waste. J Environ Manag v. 306, 114473. https://doi.org/10.1016/J.JENVMAN.2022.114473.
[74] Wang, L., Cho, D.W., Tsang, D.C.W., Cao, X., Hou, D., Shen, Z., et al., 2019. Green remediation of As and Pb contaminated soil using cement-free clay-based stabilization/solidification. Environ Int v. 126, 336–345. https://doi.org/10.1016/J.ENVINT.2019.02.057.
[75] Wang, L., Chen, L., Tsang, D.C.W., Guo, B., Yang, J., Shen, Z., et al., 2020. Biochar as green additives in cement-based composites with carbon dioxide curing. J Clean Prod v. 258, 120678. https://doi.org/10.1016/J.JCLEPRO.2020.120678.
[76] Wang, Q., shan, Li, J., Xue, Q., Poon, C.S., 2022. Immobilization and recycling of contaminated marine sediments in cement-based materials incorporating iron-

biochar composites. J Hazard Mater v. 435, 128971. https://doi.org/10.1016/J.JHAZMAT.2022.128971.

[77] Winnefeld, F., Lothenbach, B., 2010. Hydration of calcium sulfoaluminate cements — experimental findings and thermodynamic modelling. Cem Concr Res v. 40, 1239–1247. https://doi.org/10.1016/J.CEMCONRES.2009.08.014.

[78] Xia, W.Y., Du, Y.J., Li, F.S., Li, C.P., Yan, X.L., Arulrajah, A., et al., 2019. In-situ solidification/stabilization of heavy metals contaminated site soil using a dry jet mixing method and new hydroxyapatite based binder. J Hazard Mater. https://doi.org/10.1016/j.jhazmat.2019.02.031.

[79] Yin, K., Ahamed, A., Lisak, G., 2018. Environmental perspectives of recycling various combustion ashes in cement production – a review. Waste Manag v. 78, 401–416. https://doi.org/10.1016/J.WASMAN.2018.06.012.

[80] Zavarin, M., et al., 2022. Community data mining approach for surface complexation database development. Environ Sci Technol v. 56, 2827–2838. https://doi.org/10.1021/ACS.EST.1C07109/ASSET/IMAGES/LARGE/ES1C07109_0006.JPEG.

[81] Zhang, Y., Labianca, C., Chen, L., De Gisi, S., Notarnicola, M., Guo, B., et al., 2021. Sustainable ex-situ remediation of contaminated sediment: a review. Environ Pollut v. 287, 117333. https://doi.org/10.1016/J.ENVPOL.2021.117333.